

A Scalable and Parallelizable Digital Twin Framework for Sustainable Sim2Real Transition of Multi-Agent Reinforcement Learning Systems

Chinmay V. Samak* , Tanmay V. Samak*  and Venkat N. Krovi 

Abstract—This work presents a sustainable multi-agent deep reinforcement learning framework capable of selectively scaling parallelized training workloads on-demand, and transferring the trained policies from simulation to reality using minimal hardware resources. We introduce AutoDRIVE Ecosystem as an enabling digital twin framework to train, deploy, and transfer cooperative as well as competitive multi-agent reinforcement learning policies from simulation to reality. Particularly, we first investigate an intersection traversal problem of 4 cooperative vehicles (Nigel) that share limited state information in single as well as multi-agent learning settings using a common policy approach. We then investigate an adversarial autonomous racing problem of 2 vehicles (FITENTH) using an individual policy approach. In either set of experiments, a decentralized learning architecture was adopted, which allowed robust training and testing of the policies in stochastic environments. The agents were provided with realistically sparse observation spaces, and were restricted to sample control actions that implicitly satisfied the imposed kinodynamic and safety constraints. The experimental results for both problem statements are reported in terms of quantitative metrics and qualitative remarks for training as well as deployment phases. We also discuss agent and environment parallelization techniques adopted to efficiently accelerate MARL training, while analyzing their computational performance. Finally, we demonstrate a resource-aware transition of the trained policies from simulation to reality using the proposed digital twin framework.

Index Terms—Multi-Agent Systems, Autonomous Vehicles, Reinforcement Learning, Digital Twins, Real2Sim, Sim2Real

I. INTRODUCTION

In the rapidly evolving landscape of connected and autonomous vehicles (CAVs), the pursuit of intelligent and adaptive driving systems has emerged as a formidable challenge. Multi-agent reinforcement learning (MARL) stands out as a promising avenue in the quest to develop autonomous vehicles capable of navigating complex and dynamic environments while considering the nature of interactions with their peers. While cooperative MARL encourages agents to collaborate and share information to achieve common objectives, competitive MARL introduces elements of rivalry and adversary among agents, where individual success may be prioritized over coordination.

Cooperative MARL [1]–[6] fosters an environment where autonomous vehicles collaborate to accomplish collective objectives such as optimizing traffic flow, enhancing safety,

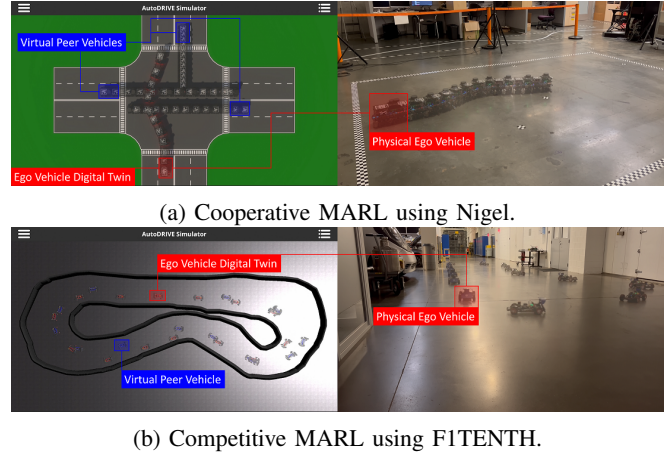


Fig. 1: Resource-aware digital twin framework for multi-agent deep reinforcement learning.

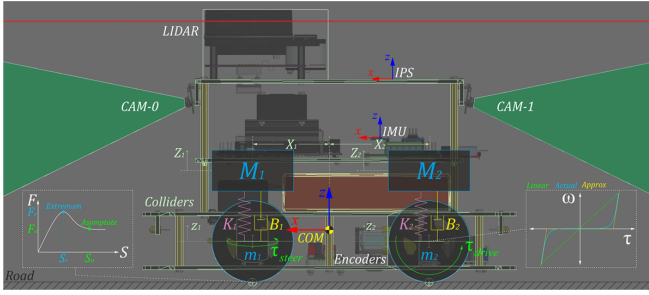
and efficiently navigating road networks. It mirrors traffic situations where vehicles must work together, such as intersection management or platooning scenarios. Challenges in cooperative MARL include coordinating vehicle actions to minimize congestion, maintaining safety margins, and ensuring smooth interactions between self-interested agents.

On the other hand, competitive MARL [7]–[10] introduces a competitive edge to autonomous driving, simulating scenarios such as overtaking, merging in congested traffic, or competitive racing. In this paradigm, autonomous vehicles strive to outperform their counterparts, vying for advantages while navigating complex and dynamic environments. Challenges in competitive MARL encompass strategic decision-making, opponent modeling, and adapting to aggressive driving behaviors while preserving safety standards.

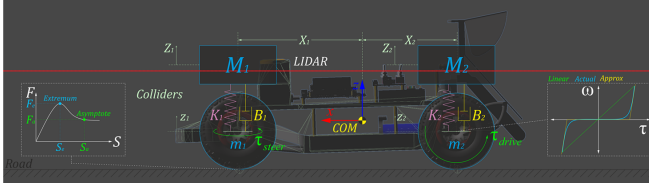
In this paper, we present AutoDRIVE Ecosystem [11], [12] as an enabler to effectively bridge the reality-to-simulation (real2sim) gap by developing physically accurate and graphically realistic digital twins of two scaled autonomous vehicles, viz. Nigel [13] and F1TENTH [14], in Section II. We then present MARL formulation, training, deployment and simulation-to-reality (sim2real) transfer for a cooperative non-zero-sum use-case of intersection traversal (refer Fig. 1(a)) in Section III, and a competitive zero-sum use-case of head-to-head autonomous racing (refer Fig. 1(b)) in Section IV. These sections also discuss the agent/environment parallelization techniques adopted to accelerate MARL training. Finally, in Section V, we present an overall summary of our work with potential future directions.

*These authors contributed equally.

C. V. Samak, T. V. Samak, and V. N. Krovi are with the Department of Automotive Engineering, Clemson University International Center for Automotive Research (CU-ICAR), Greenville, SC 29607, USA. Email: {csamak, tsamak, vkrovi}@clemson.edu



(a) Modeling and simulation of Nigel's digital twin.



(b) Modeling and simulation of F1TENTH's digital twin.

Fig. 2: Simulation of vehicle dynamics, sensors and actuators for Nigel and F1TENTH digital twins.

II. DIGITAL TWIN CREATION

In order to bridge the sim2real gap [15], we created accurate digital twin models of Nigel (refer Fig. 2(a)) as well as F1TENTH (refer Fig. 2(b)) within AutoDRIVE Simulator [16], [17] by calibrating them against their physical counterparts. The following sections only discuss the virtual vehicles, sensors, actuators, and environments adopted in this work. Further details are available in [18].

From a computing perspective, the said simulation framework was developed modularly using object-oriented programming (OOP) constructs. This allowed selectively scaling the parallel agent/environment instances on demand. Additionally, the simulator took advantage of CPU multi-threading as well as GPU instancing (only if available) to efficiently parallelize various simulation objects and processes, with cross-platform support.

A. Vehicle Dynamics Models

The vehicle model is a combination of a rigid body and a collection of sprung masses iM , where the total mass of the rigid body is defined as $M = \sum {}^iM$. The rigid body's center of mass, $X_{COM} = \frac{\sum {}^iM * {}^iX}{\sum {}^iM}$, connects these representations, with iX representing the coordinates of the sprung masses.

The suspension force acting on each sprung mass is computed as ${}^iM * {}^i\ddot{Z} + {}^iB * ({}^i\dot{Z} - \dot{z}) + {}^iK * ({}^iZ - z)$, where iZ and z are the displacements of sprung and unsprung masses, and iB and iK are the damping and spring coefficients of the i -th suspension, respectively. The unsprung mass m is also subject to gravitational and suspension forces: ${}^im * \ddot{z} + {}^iB * (\dot{z} - \dot{Z}) + {}^iK * (z - Z)$.

Tire forces are computed based on the friction curve for each tire, represented as $\begin{cases} {}^iF_{t_x} = F({}^iS_x) \\ {}^iF_{t_y} = F({}^iS_y) \end{cases}$, where iS_x and iS_y are the longitudinal and lateral slips of the i -th tire, respectively. The friction curve is approximated

using a two-piece cubic spline, defined as $F(S) = \begin{cases} f_0(S); & S_0 \leq S < S_e \\ f_1(S); & S_e \leq S < S_a \end{cases}$, where $f_k(S) = a_k * S^3 + b_k * S^2 + c_k * S + d_k$ is a cubic polynomial function. The first segment of the spline ranges from zero (S_0, F_0) to an extremum point (S_e, F_e), while the second segment ranges from the extremum point (S_e, F_e) to an asymptote point (S_a, F_a).

The tire slip is influenced by factors including tire stiffness ${}^iC_\alpha$, steering angle δ , wheel speeds ${}^i\omega$, suspension forces iF_s , and rigid-body momentum iP . These factors impact the longitudinal and lateral components of the vehicle's linear velocity. The longitudinal slip iS_x of i -th tire is calculated by comparing the longitudinal components of the surface velocity of the i -th wheel v_x with the angular velocity ${}^i\omega$ of the i -th wheel: ${}^iS_x = \frac{{}^i r * {}^i\omega - v_x}{v_x}$. The lateral slip iS_y depends on the tire's slip angle α and is determined by comparing the longitudinal v_x and lateral v_y components of the vehicle's linear velocity: ${}^iS_y = \tan(\alpha) = \frac{v_y}{|v_x|}$.

B. Sensor Models

Throttle (τ) and steering (δ) sensors are simulated using an instantaneous feedback loop. Incremental encoders are simulated by measuring the rotation of the rear wheels: ${}^iN_{ticks} = {}^iPPR * {}^iGR * {}^iN_{rev}$, where ${}^iN_{ticks}$ and iPPR respectively represent the measured ticks and base resolution (pulses per revolution) of the i -th encoder, while iGR and ${}^iN_{rev}$ respectively represent the gear ratio and output shaft revolutions of the i -th motor.

The indoor positioning system (IPS) and inertial measurement unit (IMU) are simulated based on temporally-coherent rigid-body transform updates of the vehicle $\{v\}$ w.r.t. the world $\{w\}$: ${}^wT_v = \begin{bmatrix} \mathbf{R}_{3 \times 3} & \mathbf{t}_{3 \times 1} \\ \mathbf{0}_{1 \times 3} & 1 \end{bmatrix} \in SE(3)$. IPS provides 3-DOF positional coordinates $\{x, y, z\}$ of the vehicle, while IMU supplies linear accelerations $\{a_x, a_y, a_z\}$, angular velocities $\{\omega_x, \omega_y, \omega_z\}$, and 3-DOF orientation of the vehicle as Euler angles $\{\phi_x, \theta_y, \psi_z\}$ or quaternion $\{q_0, q_1, q_2, q_3\}$.

LIDAR simulation employs iterative ray-casting $\text{raycast}\{{}^wT_l, \mathbf{R}, r_{max}\}$ for each angle $\theta \in [\theta_{min} : \theta_{res} : \theta_{max}]$ at a specified update rate. Here, ${}^wT_l = {}^wT_v * {}^vT_l \in SE(3)$ represents the relative transformation of the LIDAR $\{l\}$ w.r.t the vehicle $\{v\}$ and the world $\{w\}$, $\mathbf{R} = [\cos(\theta) \sin(\theta) 0]^T$ defines the direction vector of each ray-cast, r_{min} , r_{max} , θ_{min} and θ_{max} denote the minimum and maximum linear and angular ranges, and θ_{res} represents the angular resolution of the LIDAR. The laser scan ranges are determined by checking ray-cast hits and then applying a threshold to the minimum linear range of the LIDAR, calculated as

$$\text{ranges}[i] = \begin{cases} d_{hit} & \text{if ray}[i].hit \text{ and } d_{hit} \geq r_{min} \\ \infty & \text{otherwise} \end{cases}$$

where $\text{ray}.hit$ is a Boolean flag indicating whether a ray-cast hits any colliders in the scene, and $d_{hit} = \sqrt{(x_{hit} - x_{ray})^2 + (y_{hit} - y_{ray})^2 + (z_{hit} - z_{ray})^2}$ calculates the Euclidean distance from the ray-cast source $\{x_{ray}, y_{ray}, z_{ray}\}$ to the hit point $\{x_{hit}, y_{hit}, z_{hit}\}$.

C. Actuator Models

The driving actuators apply torque to the wheels: ${}^i\tau_{drive} = {}^iI_w * {}^i\dot{\omega}_w$, where ${}^iI_w = \frac{1}{2} * {}^im_w * {}^ir_w^2$ represents the moment of inertia, ${}^i\dot{\omega}_w$ is the angular acceleration, im_w is the mass, and ir_w is the radius of the i -th wheel. Additionally, the driving actuators simulate idle torque by applying an equivalent braking torque, i.e., ${}^i\tau_{idle} = {}^i\tau_{brake}$.

The front wheels are steered at the commanded steering angle δ using a steering actuator. The individual turning angles, δ_l and δ_r , for the left and right wheels, respectively, are computed based on the Ackermann steering geometry defined by the wheelbase l and track width w , as follows:

$$\begin{cases} \delta_l = \tan^{-1} \left(\frac{2 * l * \tan(\delta)}{2 * l + w * \tan(\delta)} \right) \\ \delta_r = \tan^{-1} \left(\frac{2 * l * \tan(\delta)}{2 * l - w * \tan(\delta)} \right) \end{cases}$$

D. Environment Models

Simulated environments can be developed using AutoDRIVE's modular infrastructure development kit (IDK), or imported from third-party tools and open standards. Specifically, the intersection traversal scenario was designed using AutoDRIVE IDK, by configuring terrain modules, road modules, and traffic elements. On the other hand, the autonomous racing scenario was created based on the binary occupancy grid map of a real-world F1TENTH racetrack, called "Porto", using a third-party 3D modeling software, and was imported and post-processed within AutoDRIVE Simulator to make it physically and graphically "sim-ready".

These environments are simulated by conducting mesh-mesh interference detection and computing contact forces, frictional forces, momentum transfer, as well as linear and angular drag acting on all rigid bodies in the scenario.

III. COOPERATIVE MULTI-AGENT SCENARIO

Inspired by [6], this use-case encompassed both single-agent and multi-agent learning scenarios, where each agent's objective was to traverse a 4-way intersection without colliding or overstepping lane bounds. Each vehicle perceived its intrinsic states and received limited state information from its peers; no external sensing modalities were employed.

A. Problem Formulation

In *single-agent learning scenario*, only the ego vehicle learned to traverse the intersection, while peer vehicles were controlled using a randomized heuristic. Vehicles shared their states via V2V communication and were reset together, making this scenario quite deterministic.

In *multi-agent learning scenario*, all vehicles learned to traverse the intersection in a decentralized manner. Vehicles shared their states via V2V communication and were reset independently, resulting in a highly stochastic scenario.

In both the scenarios, the challenge revolved around autonomous navigation in an unknown environment. The exact structure/map of the environment was not known apriori to any agent. Consequently, this decision-making problem was framed as a partially observable Markov decision process (POMDP), which captured hidden state information through environmental observations.

B. State Space

The state space S for the intersection traversal problem could be divided into observable $s^o \subset S$ and hidden $s^h \subset S$ components. The observable component included the vehicle's 2D pose and velocity, denoted as $s_t^o = [p_x, p_y, \psi, v]_t \in \mathbb{R}^4$. The hidden component encompassed the agent's goal coordinates, represented as $s_t^h = [g_x, g_y]_t \in \mathbb{R}^2$. Thus, each agent could observe the pose and velocity of its peers (via V2V communication) but kept its goal location hidden from others. Consequently, the complete state space of an agent participating in this problem was a vector containing all observable and hidden states: $s_t = [s_t^o, s_t^h]$.

C. Observation Space

Based on the state space defined earlier, each agent, i (where $0 < i < N$), employed an appropriate subset of its sensor suite to collect observations: $o_t^i = [g^i, \tilde{p}^i, \tilde{\psi}^i, \tilde{v}^i]_t \in \mathbb{R}^{2+4(N-1)}$. This included IPS for positional coordinates $[p_x, p_y]_t \in \mathbb{R}^2$, IMU for yaw $\psi_t \in \mathbb{R}^1$, and incremental encoders for estimating vehicle velocity $v_t \in \mathbb{R}^1$.

This formulation allowed $g_t^i = [g_x^i - p_x^i, g_y^i - p_y^i]_t \in \mathbb{R}^2$ to represent the ego agent's goal location relative to itself, $\tilde{p}^i = [p_x^j - p_x^i, p_y^j - p_y^i]_t \in \mathbb{R}^{2(N-1)}$ to denote the position of every peer agent relative to the ego agent, $\tilde{\psi}^i = \psi_t^j - \psi_t^i \in \mathbb{R}^{N-1}$ to express the yaw of every peer agent relative to the ego agent, and $\tilde{v}^i = v_t^j \in \mathbb{R}^{N-1}$ to indicate the velocity of every peer agent. Here, i represented the ego agent, and $j \in [0, N-1]$ represented every other (peer) agent in the scene, with a total of N agents.

D. Action Space

The vehicles were designed as non-holonomic rear-wheel-drive models featuring an Ackermann steering mechanism. As a result, the action space of an agent comprised of longitudinal (throttle/brake) and lateral (steering) motion control commands: $a_t^i = [\tau_t^i, \delta_t^i] \in \mathbb{R}^2$. For longitudinal control, the throttle command τ_t was discretized as $\tau_t \in \{0.5, 1.0\}$, which allowed the agents to slow down if necessary. The steering command δ_t was discretized as $\delta_t \in \{-1, 0, 1\}$ to steer the agents left, straight, or right for collision avoidance.

E. Reward Function

The extrinsic reward function was defined as follows:

$$r_t^i = \begin{cases} r_{goal} & \text{if safe traversal} \\ -k_p * \|g_t^i\|_2 & \text{if traffic violation} \\ k_r * (0.001 + \|g_t^i\|_2)^{-1} & \text{otherwise} \end{cases}$$

This function rewarded each agent with $r_{goal} = +1$ for successfully traversing the intersection and penalized them proportional to their distance from the goal, represented as $k_p * \|g_t^i\|_2$, for collisions or lane boundary violations. Finally, each agent was continuously rewarded inversely proportional to its distance from the goal, thereby negotiating the sparse-reward problem. The reward (k_r) and penalty (k_p) constants were set to 0.01 and 0.425 respectively, resulting in a maximum reward/penalty of 1 per time step.

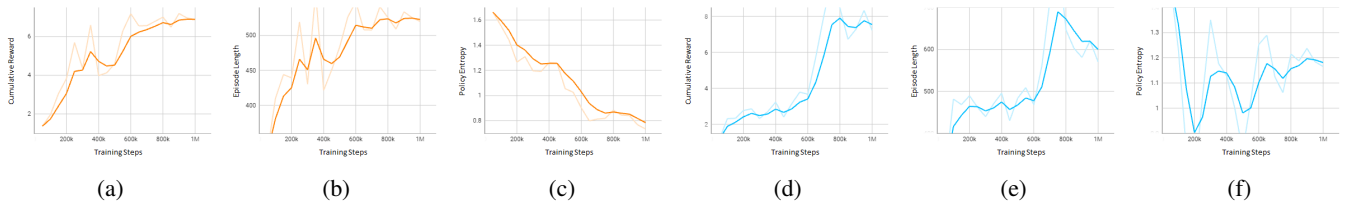


Fig. 3: Training results for (a)-(c) single-agent and (d)-(f) multi-agent intersection traversal scenarios: (a) and (d) denote cumulative reward, (b) and (e) denote episode length, while (c) and (f) denote policy entropy w.r.t. training steps.

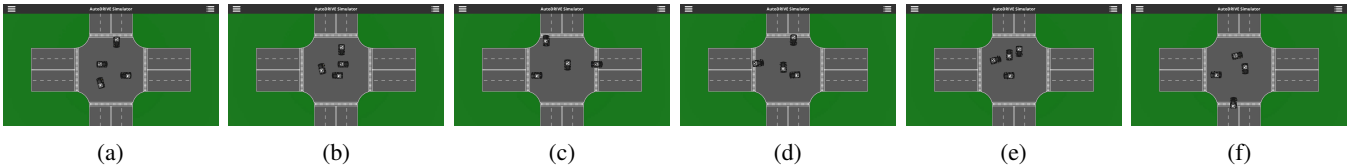


Fig. 4: Deployment results for (a)-(c) single-agent and (d)-(f) multi-agent intersection traversal scenarios: (a) and (d) denote first frozen snapshot, (b) and (e) denote second frozen snapshot, while (c) and (f) denote third frozen snapshot.

This encouraged the agents to get closer to their respective goals, reducing penalties and ultimately leading to a positive reward, r_{goal} . This approach not only expedited convergence but also restricted reward hacking.

F. Optimization Problem

The extrinsic reward function described earlier motivated each agent to maximize its expected future discounted reward $\text{argmax}_{\pi_{\theta}(a_t|o_t)} \mathbb{E} \left[\sum_{t=0}^{\infty} \gamma^t r_t \right]$ by learning a policy $\pi_{\theta}(a_t|o_t)$, which over time, transitioned into the optimal policy π^* .

G. Training

The agents were trained using an integrated machine learning (ML) framework [19] within AutoDRIVE Simulator. At each time step t , each parallelized agent i collected an observation vector o_t^i and an extrinsic reward r_t^i . Based on these inputs, it took an action a_t^i determined by the policy π_{θ} , which was recursively updated using the proximal policy optimization (PPO) algorithm [20] to maximize the expected future discounted reward.

This use-case employed a fully connected neural network (FCNN) as a function approximator for $\pi_{\theta}(a_t|o_t)$. The network had \mathbb{R}^{14} inputs, \mathbb{R}^1 outputs, and 3 hidden layers with 128 neural units each. The policy parameters $\theta \in \mathbb{R}^d$ were defined in terms of the network’s parameters.

Fig. 3 depicts key training metrics used to analyze the learning process. A general indication of “good” training is that the cumulative reward is maximized and then saturated, the episode length is adequate (longer duration implies agents wandering off in the environment, while very short duration may be indicative of agents colliding/overstepping lane bounds), and the policy entropy (i.e., randomness) has decreased steadily as the training progressed. It is to be noted that the predominant cause for the difference in trends of training metrics for single and multi-agent scenarios is the higher stochasticity of the multi-agent scenario, which is especially evident from the policy entropy.

H. Simulation Parallelization

This use-case adopted environment parallelization for accelerating the MARL training. Fig. 5(a) depicts a snapshot of 25 intersection-traversal environments training in parallel. This clearly differentiates the architecture of environment parallelization from agent/actor parallelization (refer Fig. 8(a)).

We analyzed the effect of parallelizing an intersection-traversal environment from a single instance (4 agents) up to 25 instances (100 agents) training in parallel. All the training experiments were carried out on a single laptop PC having 12th Gen Intel Core i9-12900H 2.50 GHz CPU, NVIDIA GeForce RTX 3080 Ti GPU and 32.0 GB (31.7 GB usable) RAM, with PyTorch 1.7.1 installed over CUDA 11.0.

As observed in Fig. 5(b)-(c) the reduction in training time was quite non-linear since the simulation workload increased with increasing parallelization. As a result, we can notice the curves nearly saturate after a point, which is subject to change with a different hardware/software configuration. Additionally, it should be noted that parallelization beyond a certain point can hurt, wherein the increased simulation workload may slow down the training so much that parallel policy optimization can no longer accelerate it.

I. Deployment

The trained policies were deployed onto the simulated vehicles, separately for the single-agent and multi-agent scenarios. As previously mentioned, the single-agent scenario was less stochastic, and the ego vehicle could safely traverse the intersection in most cases. In contrast, the multi-agent scenario was highly stochastic, resulting in a significantly lower success rate, especially with all vehicles navigating the intersection simultaneously.

Fig. 4(a)-(c) present three key stages of the single-agent intersection traversal scenario. The first stage depicts the ego vehicle approaching the conflict zone, where it could potentially collide with peer vehicles. The second stage

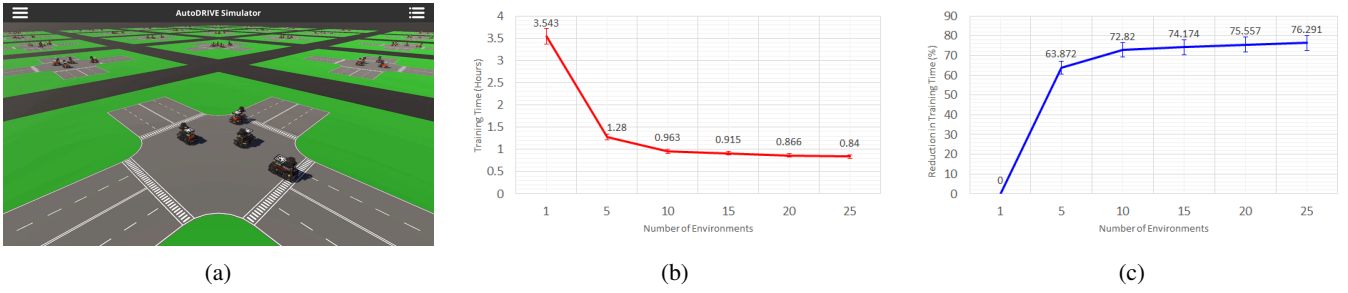


Fig. 5: Computational results for training intersection traversal scenario through environment parallelization: (a) depicts a snapshot of 25 environments training in parallel, (b) denotes the training time for different levels of environment parallelization, and (c) denotes the percentage reduction in training time for different levels of environment parallelization.

shows the vehicle executing a left turn to avoid collisions. The third stage illustrates the vehicle performing a final correction to reach its goal. Fig. 4(d)-(f) display three critical stages of the multi-agent intersection traversal scenario. In the first frame, vehicles 1 and 4 successfully avoid collision. The second frame depicts vehicle 1 finding a gap between vehicles 2 and 3 to reach its goal. In the third frame, vehicles 2 and 3 avoid collision, while vehicle 4 approaches its goal, and vehicle 1 is re-spawned.

J. Sim2Real Transfer

After simulation-based verification of the trained policies, they were transferred onto a physical vehicle, which was embedded within a true digital twin framework as depicted in Fig. 1(a) (captured at 1 Hz). Particularly, a single physical vehicle was deployed in the loop with 3 virtual vehicles, which collectively embodied the multi-agent system. The physical vehicle used LIDAR-based range flow odometry [12] for onboard state estimation (a map-based localization algorithm or a motion capture system can substitute this stage). The states of the physical vehicle were then relayed back to the simulator to update its digital twin representation in the virtual environment. The digital twin then utilized the simulation framework to establish V2X communication with its virtual peers and planned its future actions in the digital space. These action sequences were then relayed back to the physical vehicle to be executed in the real world.

This experiment validated the sim2real transferability of the trained MARL policy, without over-utilizing the hardware resources. It is worth mentioning that the digital twin framework discussed herein supports incrementally deploying multiple vehicles in the real world based on the hardware resources at disposal. Such incremental digital twin deployments can also ensure minimal physical damage, especially while deploying nascent MARL algorithms.

IV. COMPETITIVE MULTI-AGENT SCENARIO

Inspired by [9], this use-case encompassed a multi-agent learning scenario, where each agent’s objective was minimizing its lap time without colliding with the track or its opponent. Each vehicle possessed intrinsic state information and sparse LIDAR measurements; no state information was shared among the competing vehicles.

A. Problem Formulation

This use-case addressed the problem of autonomous racing in an unknown environment. The exact structure/map of the environment was not known a priori to any agent. Consequently, this decision-making problem was also framed as a POMDP, which captured hidden state information through environmental observations.

We adopted an equally weighted hybrid imitation-reinforcement learning architecture to progressively inculcate autonomous driving and racing behaviors into the agents. We hypothesized that such a hybrid learning architecture would guide the agents’ exploration, thereby reducing training time significantly. Consequently, we recorded 5 laps worth of independent demonstration datasets for each agent by manually driving the vehicles in sub-optimal trajectories.

B. Observation Space

At each time step t , the agent collected a vectorized observation: $o_t^i = [v_t^i, m_t^i] \in \mathbb{R}^{28}$. These observations were obtained using velocity estimation and exteroceptive ranging modalities mounted on the virtual vehicle(s). Here, $v_t^i \in \mathbb{R}^1$ represents the forward velocity of i -th agent, and $m_t^i = [m_t^{i,1}, m_t^{i,2}, \dots, m_t^{i,27}] \in \mathbb{R}^{27}$ is the measurement vector providing 27 range readings up to 10 meters. These readings are uniformly distributed over 270° around each side of the heading vector, spaced 10° apart.

C. Action Space

The action space to control the Ackermann-steered vehicles was defined as $a_t^i = [\tau_t^i, \delta_t^i] \in \mathbb{R}^2$. Here, $\tau_t^i \in \{0.1, 0.5, 1.0\}$ represent the discrete throttle commands at 10%, 50% and 100% PWM duty cycles for torque limited (85.6 N-m) drive actuators, and $\delta_t^i \in \{-1, 0, 1\}$ represent the discrete steering commands for left, straight, and right turns.

D. Reward Function

The agents were guided by the following signals:

- **Behavioral Cloning:** This was the core imitation learning algorithm, which updated the policy in a supervised fashion with respect to the recorded demonstrations. The behavioral cloning (BC) [21] update was carried out every once in a while, mutually exclusive of the reinforcement learning update.

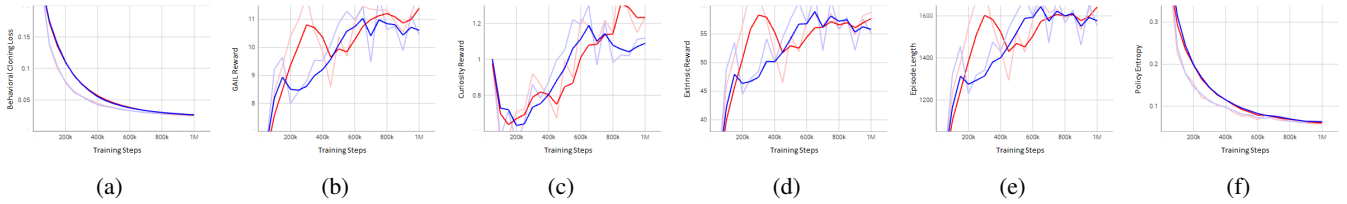


Fig. 6: Training results for multi-agent autonomous racing: (a) denotes BC loss, (b) denotes GAIL reward, (c) denotes curiosity reward, (d) denotes extrinsic reward, (e) denotes episode length, and (f) denotes policy entropy w.r.t. training steps.

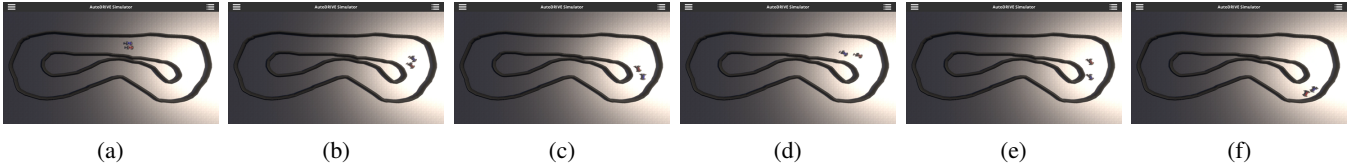


Fig. 7: Deployment results for multi-agent autonomous racing: (a)-(c) denote three frozen snapshots of a block-block-overtake sequence, and (d)-(f) denote three frozen snapshots of a let-pass-and-overtake sequence.

- **GAIL Reward:** The generative adversarial imitation learning (GAIL) reward [22] $g r_t$ ensured that the agent optimized its actions safely and ethically by rewarding proportional to the closeness of new observation-action pairs to those from the recorded demonstrations. This allowed the agent to retain its autonomous driving ability throughout the training process.
- **Curiosity Reward:** The curiosity reward [23] $c r_t$ promoted exploration by rewarding proportional to the difference between predicted and actual encoded observations. This ensured that the agent effectively explored its environment, even if the extrinsic reward was sparse.
- **Extrinsic Reward:** In the context of RL, the objectives of lap time reduction and motion constraints were handled using a novel extrinsic reward function $e r_t$, which guided the agent towards optimal behavior using the PPO algorithm [20]. The agent received a reward of $r_{checkpoint} = +0.01$ for passing each of the 19 checkpoints c_i , where $i \in [A, B, \dots, S]$ on the racetrack, $r_{lap} = +0.1$ upon completing a lap, $r_{best\ lap} = +0.7$ upon achieving a new best lap time, and a penalty of $r_{collision} = -1$ for colliding with the track bounds or peer agent (in which case both agents were penalized equally). Additionally, the agent received continuous rewards proportional to its velocity v_t , encouraging it to optimize its trajectory spatio-temporally.

$$e r_t^i = \begin{cases} r_{collision} & \text{if collision occurs} \\ r_{checkpoint} & \text{if checkpoint is passed} \\ r_{lap} & \text{if completed lap} \\ r_{best\ lap} & \text{if new best lap time is achieved} \\ 0.01 * v_t^i & \text{otherwise} \end{cases}$$

E. Optimization Problem

The task of head-to-head autonomous racing using demonstration guided reinforcement learning converged to a multi-objective problem of maximizing the expected future discounted reward by learning an optimal policy $\pi_{\theta}^*(a_t|o_t)$,

which simultaneously also minimized the behavioral cloning loss \mathcal{L}_{BC} : $\operatorname{argmax}_{\pi_{\theta}^i(a_t|o_t)} \eta \left(\mathbb{E} \left[\sum_{t=0}^{\infty} \gamma^t r_t^i \right] \right) - (1 - \eta) \mathcal{L}_{BC}$, where η is a weighting factor that controls the degree of imitation versus reinforcement learning. The cumulative reward in this case was a sum of GAIL, curiosity, and extrinsic rewards, i.e., $r_t^i = g r_t^i + c r_t^i + e r_t^i$.

F. Training

This use-case also employed a fully connected neural network (FCNN) as a function approximator for $\pi_{\theta}(a_t|o_t)$. The network had \mathbb{R}^{28} inputs, \mathbb{R}^2 outputs, and three hidden layers with 128 neural units each. The policy parameters $\theta \in \mathbb{R}^d$ were defined in terms of the network’s parameters. The policy was trained to predict throttle and steering commands directly based on collected observations, utilizing the integrated ML framework [19] within AutoDRIVE Simulator.

Fig. 6 depicts key training metrics used to analyze the learning process. A general indication of “good” training is that the behavioral cloning loss has decayed smoothly, the GAIL, curiosity, and extrinsic rewards are maximized and then saturated, the episode length is adequate (longer duration implies agents driving slowly, while very-short duration may be indicative of agents colliding without lap completion), and the policy entropy (i.e., randomness) has decreased steadily as the training progressed. It is to be noted that the non-zero offset in behavioral cloning loss indicates that the agents have not over-fit the demonstrations; rather, they have explored the state space quite well to maximize the extrinsic reward by adopting aggressive “racing” behaviors.

G. Simulation Parallelization

This use-case adopted actor/agent parallelization for accelerating the MARL training. The core actor/agent parallelization architecture involved the creation and isolation of appropriate simulation objects in different virtual “layers”. For instance, the environment was simulated on the “default” layer, whereas each family of the multi-agent

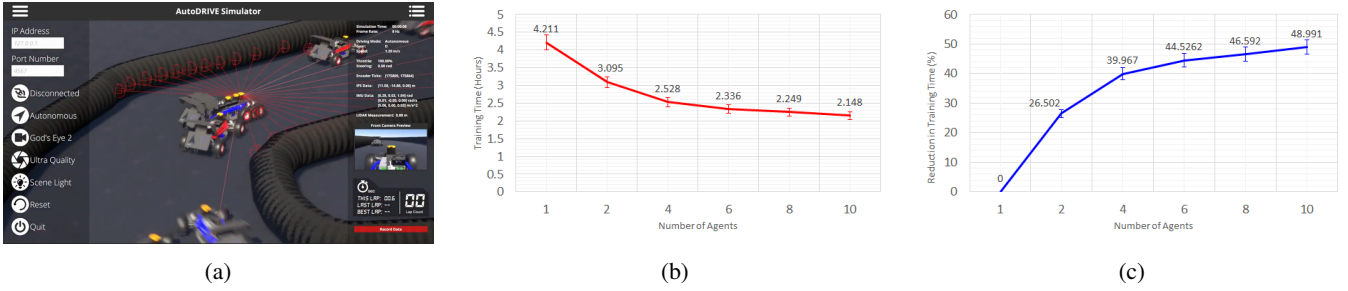


Fig. 8: Computational results for training autonomous racing scenario through actor/agent parallelization: (a) depicts a snapshot of 10×2 agents training in parallel, (b) denotes the training time for different levels of actor/agent parallelization, and (c) denotes the percentage reduction in training time for different levels of actor/agent parallelization.

system was simulated on a different layer, with the agents of the same family being simulated on the same layer. This allowed selective interactions and collision checks between specific layers of the simulation. Parallelization of perception modalities involved appropriately instantiating and isolating the interoceptive sensors (e.g., encoders, IPS, IMU, etc.) on respective layers. Exteroceptive sensors such as cameras were effectively parallelized by enabling culling mask bits only for specific layers, whereas LIDARs were parallelized by returning raycast hits only for specific layers. Fig. 8(a) depicts a snapshot of 10×2 agents training in parallel within the same environment. Notice that the agents can collide, perceive or interact only with their “true” opponents, and none of the “parallel” instances. This clearly differentiates the architecture of actor/agent parallelization from environment parallelization (refer Fig. 5(a)).

We analyzed the effect of parallelizing the 2-agent adversarial racing family from a single instance (2 agents) up to 10 such families (20 agents) training in parallel, within the same environment. All the training experiments were carried out on a single laptop PC with the same hardware and software configuration as noted in Section III-H.

As observed in Fig. 8(b)-(c) the reduction in training time was quite non-linear in this case as well. This could be primarily attributed to the increase in simulation workload with increasing parallelization. As a result, training time started saturating after a point, which is subject to change with a different hardware/software configuration. Additionally, as mentioned earlier, parallelization beyond a certain point can hurt, wherein the increased simulation workload may slow down the training so much that parallel policy optimization can no longer accelerate it.

H. Deployment

The trained policies were deployed onto the respective virtual vehicles, which were set to race head-to-head on the same track with a phase-shifted initialization (as in real F1TENTH competitions).

Fig. 7(a)-(c) present three snapshots of a block-block-overtake sequence, wherein the red agent kept blocking the blue agent throughout the straight, but the blue agent took a wider turn with higher velocity and leveraged its understeering characteristic to cut in front of the red agent and

overtake it. Fig. 7(d)-(f) display three snapshots of a let-pass-and-overtake sequence, wherein the blue agent found a gap between the red agent and inside edge of the track and opportunistically overtook it. However, due to its understeering characteristic, it went wider in the corner, thereby allowing the red agent to overtake it and re-claim the leading position.

I. Sim2Real Transfer

As highlighted in Section III-J, we first verified the ability of trained policies to complete several laps around the race track, both with and without an opponent. It was only after extensive verification, that the trained policies were transferred from simulation to reality.

The real-world experiments were conducted using a true digital twin framework (refer Fig. 1(b), captured at 1 Hz), so as to exploit the real-world characteristics of the vehicle dynamics and tire-road interconnect while being resource-altruistic by augmenting the environmental elements (e.g. race track) and peer agents (e.g. other F1TENTH vehicles) in the digital space. We utilized the Vedder electronic speed controller (VESC) based odometry to estimate the states of the physical vehicle, which were then relayed back to the simulator to update its digital twin representation in the virtual environment. The simulated 2D LIDAR on the digital twin then filled in the remaining observation space of the ego agent, which planned its future actions in the digital space. These action sequences were then relayed back to the physical vehicle to be executed in the real world.

However, in this case, owing to the requirement of agile maneuvers, it was observed that even the slightest communication latency and occasional packet drops would affect the policy to not yield the right actions at the right time. As a result, the velocity of the physical vehicle was limited to 3 m/s to account for such delays; we intend to remedy this networking-related bottleneck in the future. Nevertheless, the virtual peer vehicle operating completely in the digital space was driving at a much higher velocity limit of 10 m/s.

Finally, as described earlier, the proposed digital twin framework is flexible enough to allow adding/removing environmental components, sensor modules, and vehicles in the real world depending on the space availability and hardware resources at disposal.

V. CONCLUSION

This work presented a scalable and parallelizable multi-agent reinforcement learning framework for imbibing cooperative and competitive behaviors within autonomous vehicles. We discussed representative use-cases for each behavior type in detail, where we deliberately formulated the two problems with distinct observation spaces and reward functions, but more importantly, we also varied the learning architecture from vanilla MARL to demonstration-guided MARL. We analyzed the training metrics in each case and also noted the non-linear effect of agent/environment parallelization on the training time, with a hardware/software-specific point of diminishing return. Finally, we presented a resource-aware sim2real transfer of the trained policies using a single physical vehicle, which was plugged into the proposed digital twin framework to interact with its virtual peers within the virtual environment. Additionally, we also discussed the emerging possibilities of adapting and adopting this approach.

A natural extension to this work would be to apply the proposed approach to mid-scale and full-scale autonomous vehicles with different perception and actuation configurations. Additionally, analyzing MARL training across different types of computing platforms (both local as well as cloud computing resources) and configurations could potentially help us gain better insights from a computing perspective. Finally, innovation from the MARL front could be in the form of applying physics-informed RL to multi-agent settings for modeling agents' state transitions, formulating physics-guided reward functions, modeling and quantifying uncertainties, ensuring safety guarantees, etc.

REFERENCES

- [1] S. H. Semnani, H. Liu, M. Everett, A. de Ruiter, and J. P. How, "Multi-agent Motion Planning for Dense and Dynamic Environments via Deep Reinforcement Learning," *IEEE Robotics and Automation Letters*, vol. 5, no. 2, pp. 3221–3226, 2020.
- [2] P. Long, T. Fan, X. Liao, W. Liu, H. Zhang, and J. Pan, "Towards Optimally Decentralized Multi-Robot Collision Avoidance via Deep Reinforcement Learning," in *2018 IEEE International Conference on Robotics and Automation (ICRA)*, 2018, pp. 6252–6259.
- [3] S. Aradi, "Survey of Deep Reinforcement Learning for Motion Planning of Autonomous Vehicles," *IEEE Transactions on Intelligent Transportation Systems*, vol. 23, no. 2, pp. 740–759, 2022.
- [4] D. Wang, H. Deng, and Z. Pan, "MRCDDL: Multi-Robot Coordination with Deep Reinforcement Learning," *Neurocomputing*, vol. 406, pp. 68–76, 2020. [Online]. Available: <https://www.sciencedirect.com/science/article/pii/S0925231220305932>
- [5] X. Zhou, P. Wu, H. Zhang, W. Guo, and Y. Liu, "Learn to Navigate: Cooperative Path Planning for Unmanned Surface Vehicles Using Deep Reinforcement Learning," *IEEE Access*, vol. 7, pp. 165 262–165 278, 2019.
- [6] K. Sivanathan, B. K. Vinayagam, T. Samak, and C. Samak, "Decentralized Motion Planning for Multi-Robot Navigation using Deep Reinforcement Learning," in *2020 3rd International Conference on Intelligent Sustainable Systems (ICISS)*, 2020, pp. 709–716. [Online]. Available: <https://doi.org/10.1109/ICISS49785.2020.9316033>
- [7] F. Fuchs, Y. Song, E. Kaufmann, D. Scaramuzza, and P. Dürri, "Super-Human Performance in Gran Turismo Sport Using Deep Reinforcement Learning," *IEEE Robotics and Automation Letters*, vol. 6, no. 3, pp. 4257–4264, 2021.
- [8] Y. Song, H. Lin, E. Kaufmann, P. Dürri, and D. Scaramuzza, "Autonomous Overtaking in Gran Turismo Sport Using Curriculum Reinforcement Learning," in *2021 IEEE International Conference on Robotics and Automation (ICRA)*, 2021, pp. 9403–9409.
- [9] C. V. Samak, T. V. Samak, and S. Kandhasamy, "Autonomous Racing using a Hybrid Imitation-Reinforcement Learning Architecture," 2021. [Online]. Available: <https://arxiv.org/abs/2110.05437>
- [10] J. Betz, H. Zheng, A. Liniger, U. Rosolia, P. Karle, M. Behl, V. Krovi, and R. Mangharam, "Autonomous Vehicles on the Edge: A Survey on Autonomous Vehicle Racing," *IEEE Open Journal of Intelligent Transportation Systems*, vol. 3, pp. 458–488, 2022.
- [11] T. Samak, C. Samak, S. Kandhasamy, V. Krovi, and M. Xie, "AutoDRIVE: A Comprehensive, Flexible and Integrated Digital Twin Ecosystem for Autonomous Driving Research & Education," *Robotics*, vol. 12, no. 3, p. 77, May 2023. [Online]. Available: <http://dx.doi.org/10.3390/robotics12030077>
- [12] T. V. Samak and C. V. Samak, "AutoDRIVE - Technical Report," 2022. [Online]. Available: <https://doi.org/10.48550/arXiv.2211.08475>
- [13] C. Samak, T. Samak, and V. Krovi, "Towards Mechatronics Approach of System Design, Verification and Validation for Autonomous Vehicles," in *2023 IEEE/ASME International Conference on Advanced Intelligent Mechatronics (AIM)*, 2023, pp. 1208–1213. [Online]. Available: <https://doi.org/10.1109/AIM46323.2023.10196233>
- [14] M. O'Kelly, V. Sukhil, H. Abbas, J. Harkins, C. Kao, Y. V. Pant, R. Mangharam, D. Agarwal, M. Behl, P. Burgio, and M. Bertogna, (2019) F1/10: An Open-Source Autonomous Cyber-Physical Platform. [Online]. Available: <https://arxiv.org/abs/1901.08567>
- [15] C. V. Samak, T. V. Samak, and V. Krovi, "Towards Sim2Real Transfer of Autonomy Algorithms using AutoDRIVE Ecosystem," 2023. [Online]. Available: <https://doi.org/10.48550/arXiv.2307.13272>
- [16] T. V. Samak, C. V. Samak, and M. Xie, "AutoDRIVE Simulator: A Simulator for Scaled Autonomous Vehicle Research and Education," in *2021 2nd International Conference on Control, Robotics and Intelligent System*, ser. CCRIS'21. New York, NY, USA: Association for Computing Machinery, 2021, p. 1–5. [Online]. Available: <https://doi.org/10.1145/3483845.3483846>
- [17] T. V. Samak and C. V. Samak, "AutoDRIVE Simulator - Technical Report," 2022. [Online]. Available: <https://doi.org/10.48550/arXiv.2211.07022>
- [18] T. V. Samak, C. V. Samak, and V. N. Krovi, "Towards Validation of Autonomous Vehicles Across Scales using an Integrated Digital Twin Framework," 2024. [Online]. Available: <https://doi.org/10.48550/arXiv.2402.12670>
- [19] A. Juliani, V.-P. Berges, E. Teng, A. Cohen, J. Harper, C. Elion, C. Goy, Y. Gao, H. Henry, M. Mattar, and D. Lange, "Unity: A General Platform for Intelligent Agents," 2018. [Online]. Available: <https://arxiv.org/abs/1809.02627>
- [20] J. Schulman, F. Wolski, P. Dhariwal, A. Radford, and O. Klimov, "Proximal policy optimization algorithms," 2017. [Online]. Available: <https://arxiv.org/abs/1707.06347>
- [21] M. Bain and C. Sammut, "A Framework for Behavioural Cloning," in *Machine Intelligence 15*, 1995.
- [22] J. Ho and S. Ermon, "Generative Adversarial Imitation Learning," in *Proceedings of the 30th International Conference on Neural Information Processing Systems*, ser. NIPS'16. Red Hook, NY, USA: Curran Associates Inc., 2016, p. 4572–4580.
- [23] D. Pathak, P. Agrawal, A. A. Efros, and T. Darrell, "Curiosity-Driven Exploration by Self-Supervised Prediction," in *Proceedings of the 34th International Conference on Machine Learning - Volume 70*, ser. ICML'17. JMLR.org, 2017, p. 2778–2787.